nature materials

LETTERS

PUBLISHED ONLINE: 1 DECEMBER 2014 | DOI: 10.1038/NMAT4144

Isolated electron spins in silicon carbide with millisecond coherence times

David J. Christle[1,2], Abram L. Falk[1], Paolo Andrich[1,2], Paul V. Klimov[1,2], Jawad Ul Hassan[3], Nguyen T. Son[3], Erik Janzén[3], Takeshi Ohshima[4] and David D. Awschalom[1,2]*

The elimination of defects from SiC has facilitated its move to the forefront of the optoelectronics and power-electronics industries[1]. Nonetheless, because certain SiC defects have electronic states with sharp optical and spin transitions, they are increasingly recognized as a platform for quantum information and nanoscale sensing[2–16]. Here, we show that individual electron spins in high-purity monocrystalline 4H-SiC can be isolated and coherently controlled. Bound to neutral divacancy defects[2,3], these states exhibit exceptionally long ensemble Hahn-echo spin coherence times, exceeding 1 ms. Coherent control of single spins in a material amenable to advanced growth and microfabrication techniques is an exciting route towards wafer-scale quantum technologies.

The control of isolated electron spins is a promising basis for an array of new technologies, ranging from quantum communication[17] to nanoscale nuclear magnetic resonance[18,19] and intracellular sensing of magnetic, electric and thermal fields[20,21]. By exploiting spin-dependent optical transitions, optically detected magnetic resonance (ODMR) has proved to be a powerful technique for achieving single-spin addressability in the solid state[22,23]. As with the diamond nitrogen-vacancy centre[17–20,23], a particular focus of such research, the neutral divacancy in SiC has a spin-triplet electronic ground state[2,3] that can be polarized and read out with ODMR (refs 6,8,11,13,24–26).

In contrast to nitrogen-vacancy centres in diamond, which are addressable at visible wavelengths, divacancies in SiC are addressable in the near infrared[3,25], making their applicability to photonics and communication particularly strong. However, ODMR has previously been used in SiC only to measure spin ensembles, not individual electronic spin states. Here, by showing that neutral divacancies in SiC are both highly coherent and individually addressable, our results open new avenues for engineering high-performance electronic devices incorporating single-spin sensors and memories.

Achieving single-centre addressability with ODMR requires a nearly defect-free substrate, such that multiple defects do not occupy a diffraction-limited confocal volume. Towards this end, we use hot-wall chemical vapour deposition to grow a 120-μm-thick single-crystal epitaxial film on an n-type 4H–SiC substrate[27]. This growth technique can be used to create commercial quality, multilayer electronic structures at the wafer scale. Our epilayer is optimized to have no basal plane dislocations or polytype inclusions, and, in addition, a very low (5×10^{13} cm^{-3}) unintentional dopant density. After mechanically separating the epilayer from the substrate, we polish and dice it, and then irradiate the diced samples with 2 MeV electrons at a range of fluences (5×10^{12} cm^{-2} to 1×10^{15} cm^{-2}) to create Si and C vacancies. Finally, we anneal the samples to activate vacancy migration and form divacancies[11,26].

To measure the photoluminescence from single divacancies, we integrate a high-quantum-efficiency superconducting nanowire single-photon detector into a home-built confocal microscopy set-up that uses a 975-nm continuous-wave excitation laser. With the sample cooled to 20 K, we observe distinct bright spots (3–5 kcts s^{-1}) in a scanning photoluminescence image (Fig. 1a). We then use Hanbury Brown–Twiss interferometry to measure the second-order intensity correlation function ($g^{(2)}$) of the emission from several of these spots, all of which exhibit photon antibunching behaviour to varying degrees. The three divacancies presented in the main text of this work exhibit $g^{(2)}(t=0) < 0.5$, where t is the time delay between successive photons, indicating that they are single quantum emitters (Fig. 1b). The characteristic times of the $g^{(2)}(t)$ dips range from 9 to 12 ns, slightly less than the optical lifetimes of the neutral divacancies (14 ± 3 ns)[13], as expected from an optically pumped emitter.

Because there are two inequivalent lattice sites for C and Si atoms in 4H–SiC, namely the hexagonal (h) and quasi-cubic (k) sites, four inequivalent neutral divacancies can exist. The three we have isolated and identified in the present work are the (hh), (kk), and (kh) divacancy forms (Fig. 1c). We have observed the (hk) form in previous ensemble studies of other 4H–SiC wafers[6,11,13], but neither ensemble photoluminescence spectroscopy (Supplementary Information) nor confocal photoluminescence measurements show this form in the substrates prepared for this study.

We measure single-spin, continuous-wave ODMR spectra by sweeping the frequency (f) of an applied microwave driving field and measuring the change in photoluminescence from individual divacancies (Fig. 2a). Spin-selective transitions cause the emitted photoluminescence intensity to depend on the divacancy's spin-sublevel occupation[6,8,11]. Therefore, the photoluminescence intensity has a peak or a dip when f is resonant with a spin transition.

Each inequivalent divacancy is addressable at characteristic spin-resonance frequencies. For the c-axis-oriented (hh) and (kk) divacancies, we measure ODMR with an applied c-axis-oriented magnetic field (B) to lift the degeneracy of the $m_s = \pm 1$ spin transitions. For the (kh) defect, we measure ODMR at $B = 0$, because the crystal field already splits the degeneracy between all three spin sublevels of the basal-plane-oriented defects. ODMR on an additional (kk) divacancy that is hyperfine coupled to a nearby ^{29}Si nucleus is shown in the Supplementary Information[3].

In addition to continuous-wave ODMR measurements, we use pulsed ODMR to quantify the SiC divacancies' coherence times and spin visibility, defined as the fractional change in

[1]Institute for Molecular Engineering, University of Chicago, Chicago, Illinois 60637, USA. [2]Department of Physics, University of California, Santa Barbara, California 93106, USA. [3]Department of Physics, Chemistry and Biology, Linköping University, SE-58183 Linköping, Sweden. [4]Japan Atomic Energy Agency, 1233 Watanuki, Takasaki, Gunma 370-1292, Japan. *e-mail: awsch@uchicago.edu

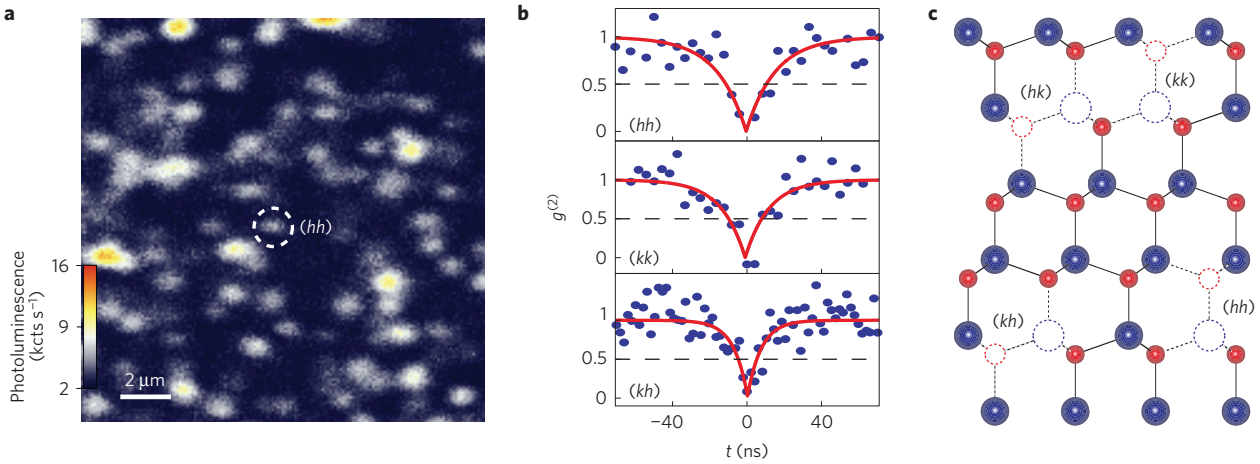

Figure 1 | Isolation of neutral divacancies in SiC. a, A 16 μm×16 μm confocal photoluminescence image from a 4H-SiC membrane irradiated at 10^{13} cm^{-2} fluence. Confocal photoluminescence is collected at a depth of 20 μm into the membrane, and the sample temperature is held at 20 K. The photoluminescence spots are almost all identified as divacancies, but not all spots are isolated single defects. **b**, $g^{(2)}(t)$ measurements for single defects of the (*hh*) (circled in **a**), (*kk*), and (*kh*) divacancy forms. The $g^{(2)}$ curves (blue dots) show strong antibunching, clearly achieving the $g^{(2)}(t=0)<0.5$ threshold for single optical emitters. The red curves are fits to a simple two-level model (details presented in the Supplementary Information). **c**, Divacancies in 4H-SiC consist of neighbouring Si and C vacancies. Because either the *h* or *k* lattice site can be vacant, there are four inequivalent forms of divacancy in 4H-SiC.

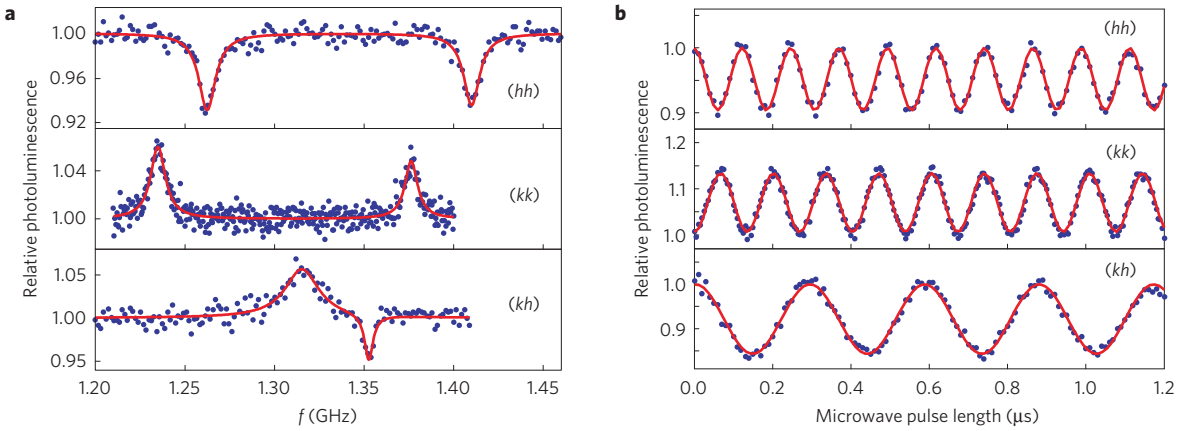

Figure 2 | Coherent control of single divacancy spins. a, Measurements of continuous-wave ODMR (blue dots) of the single divacancies from Fig. 1. The measured (*hh*) divacancy is circled in Fig. 1a. For the measurements on the (*hh*) and (*kk*) divacancies, a *c*-axis-oriented magnetic field of $B=50$ G is applied to lift the $m_s=\pm1$ degeneracy at $B=0$. For the (*kh*) divacancy, no external *B* is applied. The sample temperature is 20 K. The relative photoluminescence is the fractional change in photoluminescence arising from microwave irradiation. The background photoluminescence is subtracted before computing the relative photoluminescence. The three curves are vertically offset, for clarity, and the red curves are fits to Lorentzians. **b**, Rabi oscillations (blue dots) of the three divacancies measured in **a**, demonstrating coherent control of single electron spins in SiC. The fits (red curves) are to single sinusoids.

photoluminescence when a spin is flipped. We observe coherent Rabi oscillations of the single divacancies by applying variable-length bursts of resonant microwaves between short initialization and readout laser pulses (Fig. 2b). These oscillations are the simplest demonstration of coherent control of the spin within a two-level subspace of its spin-1 ground state. From these measurements, we infer that single divacancies have an ODMR visibility of 9–15%. Although this visibly is roughly half that of nitrogen-vacancy centres in diamond, resonant excitation techniques may be applied in the future to significantly enhance it.

Long spin-dephasing timescales are critical to both quantum information and sensing applications of isolated solid-state spins. To measure the inhomogeneous spin-dephasing time (T_2^*), we apply Ramsey pulse sequences to the isolated divacancies (Fig. 3a). For the (*hh*) and (*kh*) forms, the multi-frequency oscillations observed in the Ramsey signal (0.5–1.5 MHz) as a function of free precession time (t_{free}) are due to a weak hyperfine interaction between the divacancy electron spin and a nearby nuclear spin. As a consequence of the better homogeneity of single spins over ensembles, the inferred T_2^* times, which range from 1.1 to 4.4 μs, are significantly longer than those previously measured in ensembles[6].

To measure the homogeneous spin coherence time (T_2) of the isolated divacancies, we apply standard Hahn-echo sequences to refocus the spin coherence. We observe collapses and revivals of the coherence of a single (*kk*) divacancy as a function of t_{free} (Fig. 3b), an effect known as electron spin echo envelope modulation (ESEEM; ref. 28). The ESEEM oscillations originate from periodic spin dephasing and rephasing due to the Larmor precession of naturally abundant, spin-1/2 ^{29}Si and ^{13}C nuclei in the sample. The apparent decay of coherence in Fig. 3b is actually due to beating between these precessional frequencies—at later free evolution times, the coherence will rephase. However,

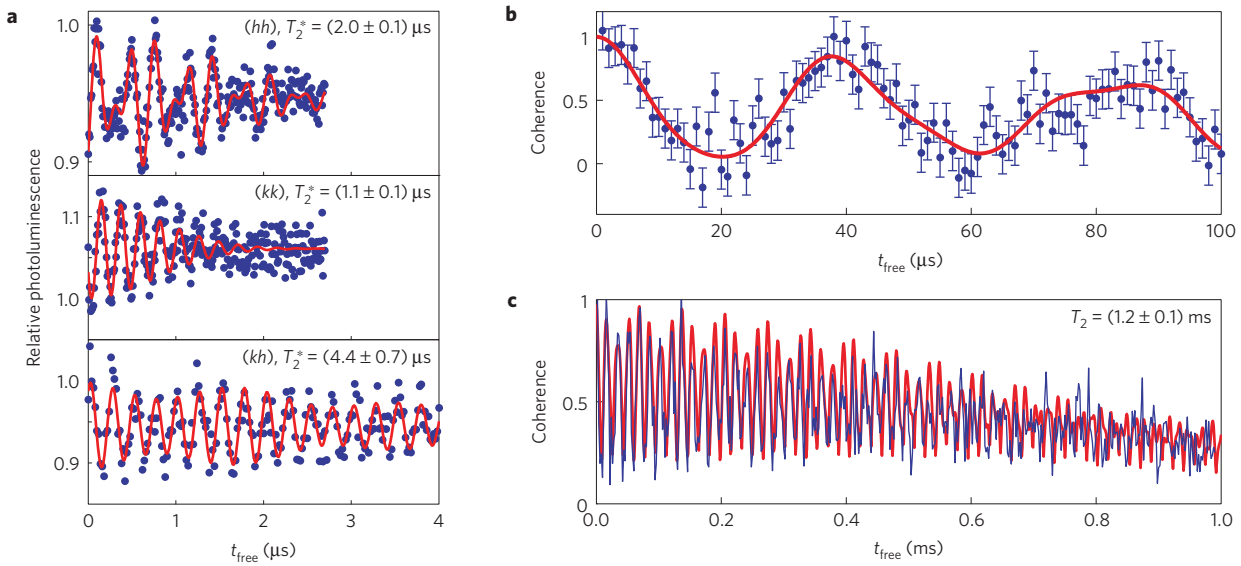

Figure 3 | Spin coherence of SiC divacancies. a, Measurements of Ramsey spin coherence of single divacancies (blue dots) at 20 K, along with a fit to an ESEEM model (red line, Supplementary Information). The fits are Gaussian decaying exponentials (with characteristic decay time T_2^*), accounting for dephasing, multiplied by sinusoids. The oscillations are due to the 4 MHz microwave detuning we used for the measurement, and the beating in the (*hh*) and (*kh*) measurements indicates weak (0.5–1.5 MHz) hyperfine coupling to nearby nuclei. **b**, A measurement of Hahn-echo spin coherence of a single (*kk*) divacancy at $B = 116$ G (blue dots). The ESEEM oscillations are due to periodic spin dephasing from the bath of naturally abundant, spin-1/2 ^{29}Si and ^{13}C nuclei, which are precessing at their Larmor frequencies. A single-spin ESEEM model (red curve, Supplementary Information) of sinusoids at these frequencies that assumes no decay (as T_2 is much longer than 100 μs) accurately reproduces the data we observe. Error bars show the standard error of the mean. **c**, A measurement (blue curve) of the Hahn-echo spin coherence of a (*kk*)-divacancy ensemble, from the 4H–SiC membrane irradiated at the highest fluence of 10^{15} cm^{-2}. The fit (red curve) is to an ESEEM model (Supplementary Information) based on the Larmor precession of the ^{29}Si and ^{13}C nuclei and a general compressed exponential decoherence function of the form $e^{-(t_{free}/T_2)^n}$, where T_2 and n are free parameters. The fit yields $T_2 = (1.2 \pm 0.1)$ ms and $n = (2.0 \pm 0.3)$. Interference effects cause the amplitude of the ESEEM oscillations to decay more quickly than the overall coherence.

limitations to the photoluminescence collection efficiency of our present apparatus (see Methods for explanation) make it practical to measure single-spin Hahn-echo signals only out to approximately $t_{free} = 100$ μs, which is shorter than the T_2 time of 4H–SiC divacancies[11]. To obtain a lower bound for the average single-spin T_2 time in our samples, we applied the same Hahn-echo sequence to an ensemble of (*kk*) divacancies. We fit the ensemble coherence data to a general ESEEM/decoherence model (Supplementary Information) to find that $T_2 = (1.2 \pm 0.1)$ ms. This T_2 time is significantly longer than the 360 μs T_2 time previously reported for divacancies in SiC (ref. 11).

Notably, although ^{29}Si is more abundant than ^{13}C (4.7% versus 1.1% natural abundance), this T_2 time is twice as long as the highest reported (600 μs) T_2 time measured for nitrogen-vacancy centres in chemically but not isotopically purified diamond[29], where the nuclear bath contains ^{13}C nuclei only. We do not completely understand the origin of these high T_2 times. However, one factor underlying them may be that the ^{29}Si and ^{13}C nuclei form separate spin baths that do not resonantly interact with each other. We expect isotopic purification and dynamical decoupling sequences to extend T_2 times in SiC even further.

Incorporating highly coherent single electron spins into high-performance SiC devices should provide many new opportunities for advancing quantum control. Along with our demonstration of coherent control of single divacancies in SiC, another work in this same issue of Nature Materials demonstrates coherent control of another intrinsic defect in SiC, the silicon vacancy[30]. Together, these works show that SiC is a versatile host for single-spin electronics. In the future, spin–photon entanglement in SiC could offer a promising route towards quantum-repeater networks, facilitated by the divacancy emission near telecom wavelengths. Moreover, spins embedded into SiC transistors could lead to electrically gated spin–spin coupling via charge-state manipulation, while spins within high-Q SiC micromechanical resonators could be a platform for studying spin–phonon interactions. Just as the performance of commercial SiC electronics has been improved by a greater understanding of defect science, future avenues for defect-based quantum technologies may be driven by SiC devices.

Methods

Spin Hamiltonian. The spin Hamiltonian describing the electronic spin-triplet ground state of the neutral divacancies in SiC is:

$$H = g\mu_B \mathbf{B}\cdot\mathbf{S} + DS_z^2 - E\left(S_x^2 - S_y^2\right) + \Sigma_j \mathbf{S}\cdot\mathbf{A}_j\cdot\mathbf{I}_j$$

where the defect axis is aligned along $\mathbf{z}$, $g = 2.0$ is the electron g-factor, μ_B is the Bohr magneton, $\mathbf{B}$ is the external magnetic field, $\mathbf{S}$ is the vector of electron spin operators, $\mathbf{I}_j$ is the vector of nuclear spin operators for the jth nearby nucleus whose hyperfine tensor is $\mathbf{A}_j$, and D and E are the crystal-field splittings. The first term of the Hamiltonian represents the electron's Zeeman interaction, the second and third terms the crystal-field interaction, and the fourth term the hyperfine interaction between the electron and nearby nuclei. The (*kk*) and (*hh*) divacancy forms are aligned along the c-axis of the crystal, and exhibit C_{3v} symmetry with $E = 0$. The (*hk*) and (*kh*) forms exhibit a lower C_{1h} symmetry with non-zero E.

Sample preparation. A 120-μm-thick epilayer of single-crystal 4H–SiC was grown on an on-axis 4H–SiC substrate[27]. The samples were irradiated at room temperature with 2 MeV electrons from a Cockcroft–Walton accelerator, creating Si and C vacancies. A 750 °C anneal for 30 min in Ar gas caused the vacancies to migrate and form vacancy complexes, including divacancies[26]. The diced silicon carbide samples were cleaned with acetone and isopropanol, followed by a deionized water rinse. Remaining surface contaminants were removed using a 3:1 mixture of concentrated sulphuric acid and hydrogen peroxide heated to 90 °C for 30 min.

Near-infrared confocal ODMR. All experiments were performed in a Janis ST-500 liquid helium flow cryostat at a temperature of 20 K. A 975-nm laser was used to non-resonantly excite the divacancy defects through their phonon

absorption sidebands. The SiC membranes were mounted on top of an antenna consisting of a short-terminated coplanar waveguide made from patterned Au on a duroid substrate. Our home-built confocal microscope used a 0.85 NA 100× near-infrared objective (Olympus, LCPLN100XIR) to focus the excitation light and collect the emitted photoluminescence. The excitation power was 1 mW at the back of the objective. The photoluminescence was filtered to collect only between 1.1 μm and 1.6 μm and was then focused into a single-mode fibre that served as the confocal pinhole. A commercial closed-cycle NbTiN superconducting nanowire single-photon detector (SingleQuantum, EOS) with approximately 28% quantum efficiency was used to register the near-infrared photons, and the antibunching measurements used a time-correlated photon counting card (PicoQuant, PicoHarp PH300) to collect the conditional photon statistics. The GHz microwaves used for spin-resonance experiments were generated by a signal generator (National Instruments, PXIe-5652) and then amplified (MiniCircuits, ZHL-30W-252) before reaching the antenna. A diagram of the experimental set-up is given in the Supplementary Information.

Our photon-detection module has a quantum efficiency of about 28%. In comparison, a typical silicon avalanche photodiode (APD) has a quantum efficiency of roughly 65% in the visible spectral range. For compatibility with our detector, we coupled the photoluminescence into a single-mode fibre (8 μm core), which also introduced additional losses of around 30–50%. Last, because the surfaces of our samples exhibited high background photoluminescence related to polishing artefacts, we needed to focus fairly deep (∼20 μm) into the SiC surface to observe isolate single emitters. From similar measurements in diamond, we estimate that the added distortions at these depths cause an additional 10–30% loss of photoluminescence. These losses are sufficient to explain the low count rates we observe relative to a comparable apparatus measuring diamond nitrogen vacancies (3–5 kcts s^{-1} versus 20 kcts s^{-1}), and straightforward routes to moderate them can be taken in the future.

Data analysis. The measurements of continuous-wave spin resonance and Rabi oscillations are background-corrected by subtracting the photoluminescence from the substrate outside of the confocal spot. This background consists of roughly 40% of the photoluminescence signal. The antibunching measurements are rebinned to a larger bin size for visual clarity, but the inferred depth of the dip from a fit to these data can be slightly skewed as an artefact of this process. To mitigate this artefact, we derived the plotted fits from a Bayesian approach applied to the raw data alone (Supplementary Information). This technique takes into account the Poisson error in each bin and infers only estimates and error bars that are physically realizable ($g^2(t=0) \geq 0$). These measurements are also background-corrected, where the background is measured about 1.2 μm away from the centre of the photoluminescence.

Received 27 June 2014; accepted 20 October 2014; published online 1 December 2014

References

1. Saddow, S. E. & Agarwal, A. K. *Advances in Silicon Carbide Processing and Applications* (Artech House, 2004).
2. Baranov, P. G. *et al.* EPR identification of the triplet ground state and photoinduced population inversion for a Si–C divacancy in silicon carbide. *JETP Lett.* **82,** 441–443 (2005).
3. Son, N. T. *et al.* Divacancy in 4H–SiC. *Phys. Rev. Lett.* **96,** 055501 (2006).
4. Tol, J. v. *et al.* High-field phenomena of qubits. *Appl. Magn. Reson.* **36,** 259–268 (2009).
5. Weber, J. R. *et al.* Quantum computing with defects. *Proc. Natl Acad. Sci. USA* **107,** 8513–8518 (2010).
6. Koehl, W. F., Buckley, B. B., Heremans, F. J., Calusine, G. & Awschalom, D. D. Room temperature coherent control of defect spin qubits in silicon carbide. *Nature* **479,** 84–87 (2011).
7. Baranov, P. G., Bundakova, A. P. & Soltamov, A. A. Silicon vacancy in SiC as a promising quantum system for single-defect and single-photon spectroscopy. *Phys. Rev. B* **83,** 125203 (2011).
8. Gali, A. Time-dependent density functional study on the excitation spectrum of point defects in semiconductors. *Phys. Status Solidi B* **248,** 1337–1346 (2011).
9. Riedel, R. *et al.* Resonant addressing and manipulation of silicon vacancy qubits in silicon carbide. *Phys. Rev. Lett.* **109,** 226402 (2012).
10. Soltamov, V. A., Soltamova, A. A., Baranov, P. G. & Proskuryakov, I. I. Room temperature coherent spin alignment of silicon vacancies in 4H– and 6H–SiC. *Phys. Rev. Lett.* **108,** 226402 (2012).
11. Falk, A. L. *et al.* Polytype control of spin qubits in silicon carbide. *Nature Commun.* **4,** 1819 (2013).
12. Klimov, P. V., Falk, A. L., Buckley, B. B. & Awschalom, D. D. Electrically driven spin resonance in silicon carbide color centers. *Phys. Rev. Lett.* **112,** 087601 (2014).
13. Falk, A. L. *et al.* Electrically and mechanically tunable electron spins in silicon carbide color centers. *Phys. Rev. Lett.* **112,** 187601 (2014).
14. Castelletto, S. *et al.* A silicon carbide room-temperature single-photon source. *Nature Mater.* **13,** 151–156 (2014).
15. Kraus, H. *et al.* Room-temperature quantum microwave emitters based on spin defects in silicon carbide. *Nature Phys.* **10,** 157–162 (2013).
16. Calusine, G., Politi, A. & Awschalom, D. D. Silicon carbide photonic crystal cavities with integrated color centers. *Appl. Phys. Lett.* **105,** 011123 (2014).
17. Bernien, H. *et al.* Heralded entanglement between solid-state qubits separated by three metres. *Nature* **497,** 86–90 (2013).
18. Mamin, H. J. *et al.* Nanoscale nuclear magnetic resonance with a nitrogen-vacancy spin sensor. *Science* **339,** 557–560 (2013).
19. Staudacher, T. *et al.* Nuclear magnetic resonance spectroscopy on a (5-nm) cubed sample volume. *Science* **339,** 561–563 (2013).
20. Toyli, D. M., Casas, C. F. d. l., Christle, D. J., Dobrovitski, V. V. & Awschalom, D. D. Fluorescence thermometry enhanced by the quantum coherence of single spins in diamond. *Proc. Natl Acad. Sci. USA* **110,** 8417–8421 (2013).
21. Kucsko, G. *et al.* Nanometre-scale thermometry in a living cell. *Nature* **500,** 54–58 (2013).
22. Wrachtrup, J., Borcyzskowski, C. v., Bernard, J., Orrit, M. & Brown, R. Optical detection of magnetic resonance in a single molecule. *Nature* **363,** 244–245 (1993).
23. Gruber, A. *et al.* Scanning confocal optical microscopy and magnetic resonance on single defect centers. *Science* **276,** 2012–2014 (1997).
24. Carlos, W. E., Glaser, E. R. & Shanabrook, B. V. Optical and magnetic resonance signatures of deep levels in semi-insulating 4H–SiC. *Physica B* **340–342,** 151–155 (2003).
25. Magnusson, B. & Janzen, E. Optical characterization of deep level defects in SiC. *Mater. Sci. Forum* **483–485,** 341–346 (2005).
26. Carlos, W. E., Graces, N. Y., Glaser, E. R. & Fanton, M. A. Annealing of multivacancy defects in 4H–SiC. *Phys. Rev. B* **74,** 235201 (2006).
27. Hassan, J., Bergman, J. P., Henry, A. & Janzén, E. On-axis homoepitaxial growth on Si-face 4H–SiC substrates. *J. Cryst. Growth* **310,** 4424–4429 (2008).
28. Oort, E. v. & Glasbeek, M. Optically detected low field electron spin echo envelope modulations of fluorescent N–V centers in diamond. *Chem. Phys.* **143,** 131–140 (1990).
29. Stanwix, P. L. *et al.* Coherence of nitrogen-vacancy electronic spin ensembles in diamond. *Phys. Rev. B* **82,** 201201 (2010).
30. Widmann, M. *et al.* Coherent control of single spins in silicon carbide at room temperature. *Nature Mater.* http://dx.doi.org/10.1038/nmat4145 (2014).

Acknowledgements

The authors thank Á. Gali, B. B. Buckley, W. F. Koehl, F. J. Heremans and G. Calusine for helpful discussions. The authors also thank S. Chemerisov and A.B. Norstel for assistance preparing preliminary samples and gratefully acknowledge support from the NSF, AFOSR MURI, the Center for Nanoscale Materials (CNM 39211), the Knut & Alice Wallenberg Foundation, the Linköping Linnaeus Initiative for Novel Functionalized Materials, the Swedish Government Strategic Research Area Grant in Materials Science (Advanced Functional Materials), and the Ministry of Education, Science, Sports and Culture of Japan, Grant-in-Aid (B) 26286047.

Author contributions

J.U.H., E.J. and N.T.S. contributed to design, growth and processing of the SiC samples. T.O. and N.T.S. contributed to electron irradiation and annealing experiments. D.J.C., A.L.F., P.A. and P.V.K. performed the optical experiments. All the authors contributed to analysis of the data, discussions and the production of the manuscript.

Additional information

Supplementary information is available in the online version of the paper. Reprints and permissions information is available online at www.nature.com/reprints. Correspondence and requests for materials should be addressed to D.D.A.

Competing financial interests

The authors declare no competing financial interests.